Supercomplexes of plant photosystem I with cytochrome b6f, light-harvesting complex II and NDH

Yadav, K N Sathish; Semchonok, Dmitry A; Nosek, Lukáš; Kouřil, Roman; Fucile, Geoffrey; Boekema, Egbert J; Eichacker, Lutz A

Published in:
Biochimica et biophysica acta

DOI:
10.1016/j.bbabio.2016.10.006

Document Version
Publisher's PDF, also known as Version of record

Publication date:
2017

Biochimica et Biophysica Acta 1858 (2017) 12–20

Contents lists available at ScienceDirect

Biochimica et Biophysica Acta

journal homepage: www.elsevier.com/locate/bbabio

Supercomplexes of plant photosystem I with cytochrome b6f, light-harvesting complex II and NDH

K.N. Sathish Yadav [a,1], Dmitry A. Semchonok [a,1], Lukáš Nosek [b], Roman Kouřil [b], Geoffrey Fucile [c,d], Egbert J. Boekema [a,*], Lutz A. Eichacker [e,**]

[a] Electron Microscopy Group, Groningen Biomolecular Sciences & Biotechnology Institute, University of Groningen, 9747 AG, Groningen, The Netherlands
[b] Department of Biophysics, Centre of the Region Haná for Biotechnological and Agricultural Research, Faculty of Science, Palacký University, 78371 Olomouc, Czech Republic
[c] Department of Molecular Biology, University of Geneva, Geneva, Switzerland
[d] Department of Plant Biology, University of Geneva, Geneva, Switzerland
[e] CORE, University of Stavanger, N-4021 Stavanger, Norway

ARTICLE INFO

Article history:
Received 19 September 2016
Received in revised form 11 October 2016
Accepted 13 October 2016
Available online 15 October 2016

Keywords:
Photosystem I
Cytochrome b_6f complex
NDH
Supercomplex
Electron microscopy

ABSTRACT

Photosystem I (PSI) is a pigment-protein complex required for the light-dependent reactions of photosynthesis and participates in light-harvesting and redox-driven chloroplast metabolism. Assembly of PSI into supercomplexes with light harvesting complex (LHC) II, cytochrome b_6f ($Cytb_6f$) or NAD(P)H dehydrogenase complex (NDH) has been proposed as a means for regulating photosynthesis. However, structural details about the binding positions in plant PSI are lacking. We analyzed large data sets of electron microscopy single particle projections of supercomplexes obtained from the stroma membrane of *Arabidopsis thaliana*. By single particle analysis, we established the binding position of $Cytb_6f$ at the antenna side of PSI. The rectangular-shaped $Cytb_6f$ dimer binds at the side where Lhca1 is located. The complex binds with its short side rather than its long side to PSI, which may explain why these supercomplexes are difficult to purify and easily disrupted. Refined analysis of the interaction between PSI and the NDH complex indicates that in total up to 6 copies of PSI can arrange with one NDH complex. Most PSI-NDH supercomplexes appeared to have 1–3 PSI copies associated. Finally, the PSI-LHCII supercomplex was found to bind an additional LHCII trimer at two positions on the LHCI side in Arabidopsis. The organization of PSI, either in a complex with NDH or with $Cytb_6f$, may improve regulation of electron transport by the control of binding partners and distances in small domains.

1. Introduction

Photosystem I (PSI) and photosystem II (PSII) are the major protein complexes regulating the light reactions of oxygenic photosynthesis. Light captured by PSI and PSII is ultimately used for the production of ATP and NADPH. Both PSI and PSII are universally distributed throughout prokaryotes and eukaryotes capable of oxygenic photosynthesis, including higher plants, macroalgae and cyanobacteria. PSI and PSII have the ability to form supercomplexes with other photosynthetic proteins, in particular with LHCII [1,2] and NDH [3]. Plant PSI can bind one LHCII trimer at the side of the PsaK and PsaL subunits [2,4,5]. This additional antenna increases the light-harvesting capacity for PSI under state transition. The additional antenna of the PSI-LHCII complex of the model green alga *Chlamydomonas reinhardtii* is composed of two LHCII trimers plus CP29 [6].

Besides light-harvesting, PSI supercomplexes are also involved in regulating electron flow. Two important modes of electron flow have been described: linear electron flow (LEF) and cyclic electron flow (CEF). In LEF, PSII, $Cytb_6f$, and PSI work in series to produce ATP and NADPH. In CEF only PSI and $Cytb_6f$ are involved as the major players, without contribution of PSII. This pathway generates extra ATP at the expense of NADPH by redirecting electron flow from PSI back to the $Cytb_6f$. Control of LEF and CEF can thus adjust the ratio of produced ATP/NADPH in response to changing metabolic and environmental conditions. Under certain conditions, CEF appears to contribute substantially to photosynthetic electron flow, for example during induction of photosynthesis and under abiotic stress such as drought, high light and extreme temperatures [7]. Currently two cyclic pathways are known that require either the PROTON GRADIENT REGULATION5 (PGR5) and PGR5-LIKE1 (PGRL1) complex [8] or the NADH dehydrogenase-like complex (NDH) [9,10]. Whereas the PGR5-dependent pathway is efficient in control of the ATP/NADPH ratio and

* Correspondence to: E.J. Boekema, Department of Electron Microscopy, Groningen Biomolecular Sciences & Biotechnology Institute, University of Groningen, Nijenborgh 9, 9747 AG Groningen, The Netherlands.
** Correspondence to: L.A. Eichacker, CORE, University of Stavanger, Richard Johnsens gate 4, N-4021 Stavanger, Norway.
E-mail addresses: e.j.boekema@rug.nl (E.J. Boekema), lutz.eichacker@uis.no (L.A. Eichacker).
[1] These authors contributed equally to this work.

http://dx.doi.org/10.1016/j.bbabio.2016.10.006
0005-2728/

essential to induce dissipation of energy by non-photochemical quenching, the NDH-dependent pathway is considered not to affect non-photochemical quenching. Rather it alleviates over-reduction of the stromal compartment and reduces photoinhibition [11]. Although, both pathways are extremely important for photoprotection and photosynthesis, recent analysis of *hcef* (high CEF) *Arabidopsis thaliana* mutants, revealed a key role of the NDH in enhanced CEF and augmenting production of ATP [12]. This is consistent with previous observations that accumulation of hydrogen peroxide in barley under photooxidative stress was found to mediate the induction of NDH and to enhance its activity [13]. These findings posit a crucial role for the NDH-pathway of cyclic electron transport in environmental stress acclimation.

How the functional and structural aspects of PSI supercomplexes contribute to regulation of electron flow is however not fully understood. Several years ago a supercomplex composed of PSI and $Cytb_6f$ complex was described in *Chlamydomonas reinhardtii* [14]. This supercomplex was proposed to play a role in CEF, but until now has not been structurally characterized. Another PSI-NDH supercomplex that appears to play a specific role in electron flow was recently described [3]. This supercomplex is composed of two PSI complexes held together by a centrally positioned NDH complex.

Despite the increasing number of tentative PSI supercomplexes, no isolation of a plant PSI-$Cytb_6f$ particle has yet been demonstrated. This stimulated us to perform a systematic search for novel supercomplexes, especially for those in which $Cytb_6f$, NDH and LHCII are involved. We used free-flow electrophoresis in combination with blue native electrophoresis (BN) and clear native (CN)-PAGE followed by mass spectrometric determination of the protein composition of isolated complexes. We demonstrate the isolation of PSI-$Cytb_6f$ supercomplexes from Arabidopsis chloroplast membranes. The chance of finding such complexes in single particle analysis was increased by mobility analysis of thylakoid protein complexes lacking the PPH1 phosphatase (PPH1) [15]. The Arabidopsis *pph1* null mutant accumulates an increased concentration of PSI-LHCII supercomplexes, associated with increased CEF [16]. We describe the PSI-$Cytb_6f$ supercomplex in *Arabidopsis* for the first time by electron microscopy (EM), and also show several novel types of PSI-LHCII supercomplexes, where additional LHCII trimers were determined next to the Lhca1–4 proteins of the standard PSI-LHCII supercomplex. In addition, we describe the structural organization of novel PSI-NDH supercomplexes identified from large EM data sets. These results indicate a higher level of organization of the unstacked grana membrane than previously considered.

2. Materials & methods

2.1. Isolation of protein complexes from thylakoid membranes

For isolation of photosystem particles, thylakoid membranes were isolated from *Arabidopsis thaliana* plants as described and aliquots corresponding to 100 μg of Chl were frozen in liquid N_2 before storage at −80 °C [17]. Thylakoid membranes corresponding to 300 μg Chl were thawed, centrifuged for 2 min at 5000 rcf and 4 °C, and membranes were suspended in TMKS buffer (25 mM tricine/NaOH pH 7.2, 5 mM $MgCl_2 \cdot 6H_2O$, 10 mM KC1, 200 mM sorbitol) at a concentration of 1 μg Chl μl^{-1}. Membranes were solubilized in TMKS using 16 mM digitonin for 10 min at 10 °C. The sample was micro-centrifuged at 25,000 rcf for 30 min at 10 °C and the supernatant was processed by interval zone free-flow electrophoresis (IZE-FFE). Samples were supplemented with 0.02% (*v*/v) of an anionic tracking dye 2-(4-sulfophenylazo)-1,8-dihydroxy-3,6-naphthalene disulfonic acid (SPADNS) (Becton Dickinson, Franklin Lakes, NJ, USA) before application to IZE-FFE and analysis of protein complexes using 2D-BN/SDS-PAGE [17].

PSI-NDH supercomplexes were co-purified with PSII megacomplexes using clear native electrophoresis (CN-PAGE) according to [18].

2.2. Interval zone free-flow electrophoresis

All IZE-FFE separations were conducted in a standard free-flow electrophoresis (FFE) system (FFE Service GmbH, Germany) with a gap size of 0.2 mm and with the following buffers. As electrode buffers 100 mM formic acid and 200 mM Bis-Tris, pH 6.4 was used at the anode and 100 mM NaOH, 200 mM glycine, pH 10 at the cathode. For anodic stabilization, a buffer composed of 100 mM HCl, 50 mM formic acid and Bis-Tris, was applied through inlet 1. Anodic stabilization was increased during the experimental period by raising the pH from 4.5 (initial) to 6.4 (final). Separation buffer 1, containing 10 mM hydroxy-isobutyric acid (HIBA), 0.2% digitonin, and adjusted to pH 5.4 with Bis-Tris, was applied through inlets 2–4; separation buffer 2, containing 10 mM HIBA, 0.2% digitonin, and adjusted to pH 6.2 with Bis-Tris, was applied through inlets 5 and 6; separation buffer 3, containing 10 mM HIBA, 5 mM NaCl, 0.2% digitonin, and adjusted to pH 7.0 with Bis-Tris, was applied through inlet 7; and separation buffer 4, containing 10 mM HIBA, and adjusted to pH 7.0 with Bis-Tris, was applied through inlet 8. At inlet 9, cathodic stabilization buffer, composed of 150 mM HIBA, and 375 mM Imidazole pH 7.45 was applied and the separation media were neutralized at the end of the separation making use of a counter-flow solution composed of 250 mM sorbitol, 50 mM Bis-Tris, and 20 mM N-(1,1-Dimethyl-2-hydroxyethyl)-3-amino-2-hydroxypropanesulfonic acid (AMPSO) pH 8.04 or 250 mM sorbitol, 10 mM HIBA, 10 mM Bis-Tris, pH 6.2. Samples were applied via inlet 7, on the cathodic side of the separation chamber.

For separation of the sample, the system was operated in a preprogrammed IZE mode at a high voltage setting of 1600 V, and 86 mA, and with the buffer flow adjusted to 40 ml/h (HV). Interval conditions for sample application and separation were as follows. Sample loading was conducted using a sample pump for 70 s at 5.2 ml/h and a pump for controlling the buffer flow rate of 120 ml/h. When the sample pump was stopped, sample transport into the field chamber was completed for an additional 20 s at 120 ml/h. During electrophoresis at HV, buffer flow rate was reduced to 40 ml/h and separation conducted within 4.5 min. Elution of separated protein complexes was performed in the absence of HV at a buffer flow of 240 ml/h and samples collected in 96 well polyethylene microtiter plates (Becton Dickinson, Franklin Lakes, NJ, USA). IZE was repeated according to the amount of material required for further analysis. Samples in microtiter plates were processed for BN-PAGE [19]. Gelbands were stained using Coomassie G250 [20].

2.3. Mass spectrometry analysis

Gel slices from the native gels were excised and transferred into a 96-well PCR plate. The gel bands were cut into 1 mm^2 pieces, destained, reduced (DTT) and alkylated (iodoacetamide) and subjected to enzymatic digestion with trypsin overnight at 37 °C. After digestion, the supernatant was pipetted into a sample vial and loaded onto an autosampler for automated LC-MS/MS analysis.

All LC-MS/MS experiments were performed using a nanoAcquity UPLC (Waters Corp., Milford, MA) system and an LTQ Orbitrap Velos hybrid ion trap mass spectrometer (Thermo Scientific, Waltham, MA). Separation of peptides was performed by reverse-phase chromatography using a Waters reverse-phase nanoLC column (BEH C18, 75 μm i.d. × 250 mm, 1.7 μm particle size) at flow rate of 300 nl/min. Peptides were initially loaded onto a pre-column (Waters UPLC Trap Symmetry C18, 180 μm i.d × 20 mm, 5 μm particle size) from the nanoAcquity sample manager with 0.1% formic acid for 3 min at a flow rate of 10 μl/min. After this period, the column valve was switched to allow the elution of peptides from the pre-column onto the analytical column. Solvent A was water + 0.1% formic acid and solvent B was acetonitrile + 0.1% formic acid. The linear gradient employed was 5–35% B in 60 min.

The LC eluent was sprayed into the mass spectrometer by means of a New Objective nanospray source. All *m*/*z* values of eluting ions were

measured in the Orbitrap Velos mass analyzer, set at a resolution of 30,000. Data dependent scans (Top 20) were employed to automatically isolate and generate fragment ions by collision-induced dissociation in the linear ion trap, resulting in the generation of MS/MS spectra. Ions with charge states of 2 + and above were selected for fragmentation. Post-run, the data was processed using Protein Discoverer (version 1.2., ThermoFisher). Briefly, all MS/MS data were converted to mgf files and these files were submitted to the Mascot search algorithm (Matrix Science, London UK) and searched against the TAIR10 database, using a fixed modification of carbamidomethyl (C) and a variable modification of oxidation (M).

2.4. Electron microscopy

For EM specimens, 4 μl of *Arabidopsis* fractions, purified by free flow electrophoresis, was applied onto glow-discharged carbon coated grids. The sample was absorbed for 1 min, excess sample was blotted with filter paper then stained with 2% uranyl acetate for enhancing the contrast. Images were collected on a Tecnai T20 (FEI, Eindhoven, NL) equipped with a LaB_6 tip operating at 200 kV. Images of 2048 × 2048 pixels were recorded at 133,000× magnification using a Gatan 4000 SP 4 K slow-scan CCD camera with a pixel size of 0.224 nm. A total of 35,000 particles were manually picked from 60,000 images and single particles were analyzed with XMIPP software [21], including alignments, statistical analysis and classification and RELION software [22]. The best class members were taken for the final class-sums. For three-dimension reconstruction, 4115 selected PSI-$Cytb_6f$ projections were processed using SCIPION protocol xmipp3-reconstruct [23].

3. Results

Free-flow electrophoresis (FFE) was employed to separate solubilized membranes into fractions of protein complexes. Separation of the protein particles by operating FFE in the IZE setup required 4.5 min and the same amount of time was used for preparation of an electron microscopy specimen. The combination of both techniques minimized the preparation time for fixation of particles and enabled examination of large fragile photosynthetic complexes and supercomplexes. Inspection of specimens by EM revealed that FFE fractions at the beginning of the separation profile (fractions 31–39, Fig. 1) contained mostly PSII complexes. Fractions 37 and 39 were highly enriched in ATP synthase, which was easily recognized due to its uniquely shaped F_0 stalk and F_1 headpiece (data not shown). Some ATP synthases were associated in small strings, as observed before [24]. We focused our efforts on the analysis of fractions containing PSI and $Cytb_6f$ (fractions 53–59), pear-shaped PSI-LHCII particles in the middle of the fractionation, and smaller particles down to the size of LHCII (fractions 47–53) (Fig. 1).

Analysis of FFE fractions by SDS-PAGE (Fig. 2A) and BN-PAGE (Fig. 2B) both corroborated the information from the EM inspection of particles. The mobility of protein complexes in the FFE separation was judged from the intensity variation of single molecular weight protein bands along the microtiter plate fractions from the anode (fraction 1) to the cathode (fraction 96). The most characteristic feature of the digitonin solubilized thylakoid extract was a continuous band at about 55 kDa, consistent with the mobility of ATPase, that was well determined in fractions 27–43 with a highest concentration between fractions 35–39 (Fig. 2A). Two higher molecular weight bands at about 98 kDa and 49 kDa indicated the presence of PSI reaction center proteins. The intensity of these bands varied in parallel with those smaller than about 20 kDa in fractions 37–57, with highest intensity in the bands between 39 and 43 and at 49. A second increase of the PSI containing fractions was determined between fractions 53–57, although an additional protein band was determined between molecular weight 28 and 38 kDa in these fractions (Fig. 2A). In order to determine the proteins assembly status, the remaining volume of about 300 μl from the microtiter plate fractions was concentrated by spin columns using a membrane with a 100 kDa cut-off. The supernatant was separated by BN-PAGE (15 h, 17.5 V per gel), and the gel-bands were visualized using colloidal Coomassie. As in SDS-PAGE, the assembly status of the protein complexes separated by FFE was judged from the intensity variation of protein bands of equal molecular weight. Three bands with the highest protein concentration were found around 700 kDa, according to the molecular weight of standard proteins (lane M, Fig. 2B). The lowest molecular weight band was determined in fractions 37/39, the highest molecular weight band in fractions 49/51, and a band with intermediate molecular weight in fractions 53–57 (Fig. 2B). A separation of the solubilized extract directly by BN-PAGE (Fig. 2B, lane S) showed that the molecular weight difference between the three bands was maintained; however, all bands were found at slightly lower molecular weight in the BN gel after FFE separation. This indicated that the mobility of the protein complexes in BN-PAGE was increased after separation by IZE-FFE. Analysis of the proteins by TEM, and the combination of the molecular weight data from the single proteins and protein complexes indicated that ATPase accumulated in fraction 37–39, while PSI-LHCII complexes accumulated in fractions 49–51, and PSI accumulated in fractions 53–57. Two bands around the 480 kDa molecular weight standard (Fig. 2B, M) were found with the same intensity distribution as the ATPase band in fraction 37–39 and the PSI band in fraction 53–57. This indicated that both ATPase and PSI were comigrating with a protein complex of lower molecular weight. In contrast, a band of a complex around the 242 kDa molecular weight standard was also overlapping with the PSI-LHCII band in fractions 49/51. However, the intensity pattern of both bands showed shifted maximum staining intensity in fractions 41–51 and in fractions 47/49 indicating that the mobility of both protein complexes was overlapping but complexes were not comigrating during FFE separation. The band pattern of the lower molecular band correlated with a 25 kDa protein band (LHCII) in SDS-PAGE (Fig. 2A). The protein was also present in fraction 29–39 in SDS-PAGE, but not detectable in the fractions after BN-PAGE. EM data also indicated the presence of PSII complexes in fractions 31–39, and BN-PAGE analysis showed the PSII bands in fractions 35–39. This indicated that the 242 kD band maxima in fraction 47–49 resembled an assembly state of LHCII that did not specifically associate with PSII or PSI; whereas, another assembly state of LHCII in fractions 31–39 remained specifically bound to the PSII complexes during FFE and BN-PAGE separation.

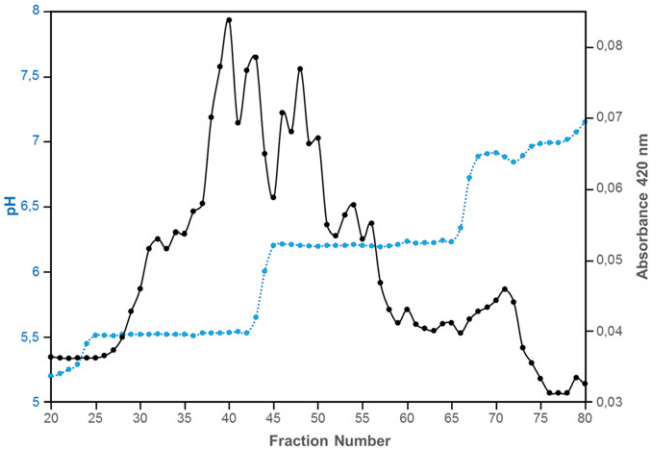

Fig. 1. Charge-based separation of *Arabidopsis thaliana* thylakoid protein complexes by IZE-FFE. Membranes corresponding to 300 μg Chl were solubilized in TMKS buffer, using digitonin (16 mM). Non-solubilized membranes were removed by centrifugation (25,000 ×*g*, 30 min) and the supernatant (100 μg Chl) was separated by IZE-FFE. Separation was conducted continuously in a buffer containing 10 mM HIBA, Bis-Tris pH 5.6 (fractions 24–44) and pH 6.2 (fractions 45–65), 200 mM sorbitol and 0.8 mM digitonin (blue dotted line). Thylakoid membrane protein complexes were collected in 300 μl fractions in a 96 well microtiter plate (Fraction number) and the localization of Chl-binding protein complexes was determined spectroscopically by measuring absorption at 420 nm (black curve).

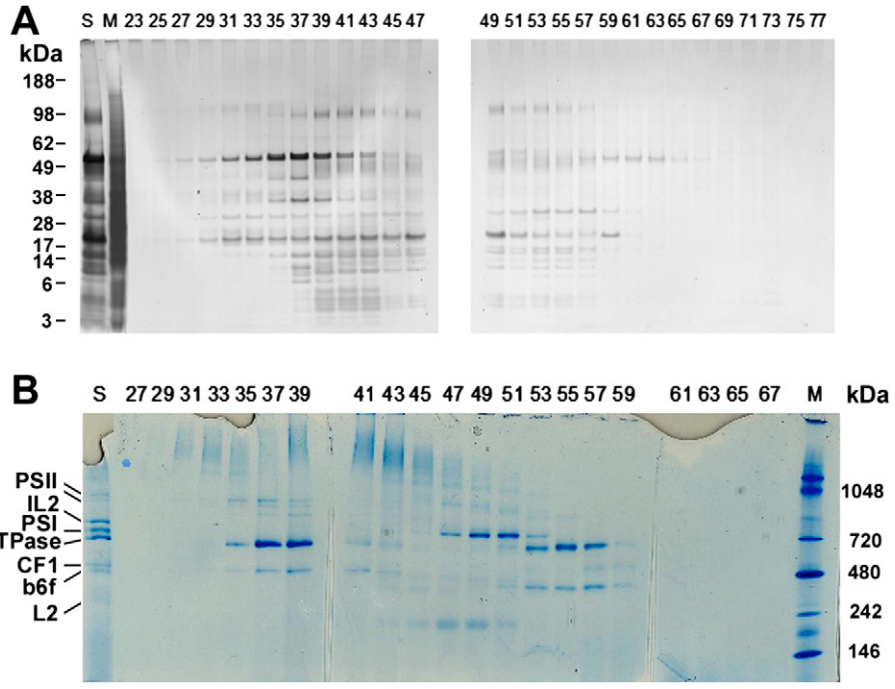

Fig. 2. Separation of proteins and protein complexes upon IZE-FFE application. (A) Solubilized thylakoid membranes were separated by IZE-FFE and 10 μl of odd numbered FFE fractions (23–77) were separated by SDS-PAGE and silver stained. (B) BN-PAGE separation of odd-number fractions 27–67. Fraction volumes were concentrated by 100 k cut-off centrifugation membranes (6 min, 13,000 ×*g*, 4 °C) and 25 μl loaded onto ready-made native 3–12% gradient gels (Invitrogen). Protein complexes separated in gel-bands were identified as photosystem II (II), photosystem I (IL2), photosystem I binding light-harvesting protein of photosystem II (L2), the ATP synthase (ATPase), the F1 domain from chloroplast ATP synthase (CF1), and the $Cytb_6f$ complex (b_6f) by mass spectrometry. Molecular weight standards (lane M) (Invitrogen, kDa) and protein complexes without IZE-FFE pre-separation (lane S) and with IZE-FFE separation (numbered lanes) were stained by colloidal Coomassie G250 and gel-bands documented by white light scanning.

3.1. Analysis of Arabidopsis PSI-Cytb$_6$f supercomplexes

The two protein bands in BN-PAGE that appeared to comigrate in FFE fractions 53–59 were analysed further. Mass spectrometry analysis was performed for the two protein bands at about 647 and 384 kDa (Supplemental Table 1). The higher molecular weight band was identified as PSI, since 85% of the identified peptides originate from specific PSI proteins. (Supplemental Table 2A). Identification of two peptides from PetA, and five peptides from the CF1 α and β subunits indicated however that despite the 2D separation, the 647 kDa band was not pure. The lower molecular weight band was identified as $Cytb_6f$ with 81% of the peptides originating from specific $Cytb_6f$ subunit proteins. Also here seven peptides were identified from PSII subunits PsbB, -C, and -D indicating that the 2D separation protocol provided a substantial enrichment of the PSI and $Cytb_6f$ complex, but the MS analysis indicated that bands were not pure. We therefore checked whether the co-mobility pattern of both protein bands in BN-PAGE was based on the destabilization of a complex composed of PSI and $Cytb_6f$ complexes by analysis of the corresponding FFE fractions by single particle analysis.

A total of 35,000 particles were picked from micrographs of FFE fractions containing PSI and $Cytb_6f$ (fractions number 53–59) and was submitted to single particle analysis including classification. Many classes showed PSI particles in a highly tilted position but in about half of all projections PSI was more or less in a top-view position, as in the membrane plane. Out of 20,000 particles in top-view projection, 4500 show a PSI-$Cytb_6f$ supercomplex in which $Cytb_6f$ is present as a dimer (classes of Fig. 3A-H). In 9500 particles, the attached $Cytb_6f$ is monomeric (Fig. 3I–K), and in the rest of the particles the $Cytb_6f$ was loosely bound (Fig. 3M–O) or completely detached from PSI upon staining (Fig. 3P). Single $Cytb_6f$ dimers were analyzed as well and a map is depicted (Fig. 3L) in a position as in the non-tilted dimer classes (Fig. 3A,B). The dimer is rectangular and the overall size and shape is comparable to the high-resolution structures determined by X-ray crystallography [25,26]. The dimer also has strong stain-excluding "bright" features, in comparison to the deeper stain-embedded PSI complex. This is related to the larger dimension of $Cytb_6f$ vertical to the membrane.

The structure of $Cytb_6f$ dimers detached from PSI (Fig. 3L) is very similar to those bound to PSI (Fig. 3A–D). However, the edges of bound dimers are rounded up as a result of a low overall resolution in these maps. A similar loss of detail is visible in a 20 Å resolution EM map of the $Cytb_6f$ complex, compared to a map at 8 Å resolution [27]. The low resolution is caused by a limited number of summed images in each class. All classes show the same supercomplex, but seen from many different angles (Fig. 3A–H). To deduce where the $Cytb_6f$ dimer is attached to PSI we calculated a low-resolution 3D model from 4115 2D projection from classes of Fig. 3A–H, see Fig. 4A, B. The model was shifted into a position compatible to the regular PSI (Fig. 4C) and the PSI-LHCII (Fig. 4D), of which we know by comparison to the high-resolution 3D model that they show PSI from the stromal side. The model can be correlated to these 2D maps because according to the high-resolution structure, the shape of $Cytb_6f$ is highly asymmetrical in respect to the membrane [25,26]. It protrudes strongly on its lumenal side and minimally on the stromal side, in contrast to PSI with its rather flat lumenal surface. This difference is reflected in the model, where the $Cytb_6f$ part of the PSI-$Cytb_6f$ supercomplex is flat on the stromal side (Fig. 4A), but substantially protruding from the lumenal side (Fig. 4B). The surface profile of PSI further confirms the position of the 3D model with respect to the 2D maps. The stromal-exposed bump on PSI, made by the PsaC, -D and -E subunits [28,29], is on the upper half of PSI (Fig. 4A), whereas the lower thinner side of the PSI model is occupied by the flat LHCI antenna proteins. Thus the model shows that in the PSI-$Cytb_6f$ supercomplex $Cytb_6f$ is bound to the left side of the light-harvesting part of PSI, where the Lhca1 subunit is located [28,29], as also depicted in a model (Fig. 7A).

3.2. Analysis of Arabidopsis PSI-LHCII supercomplexes

A set of 15,000 potential PSI-LHCII supercomplexes were selected and processed by single particle image analysis. The standard PSI-

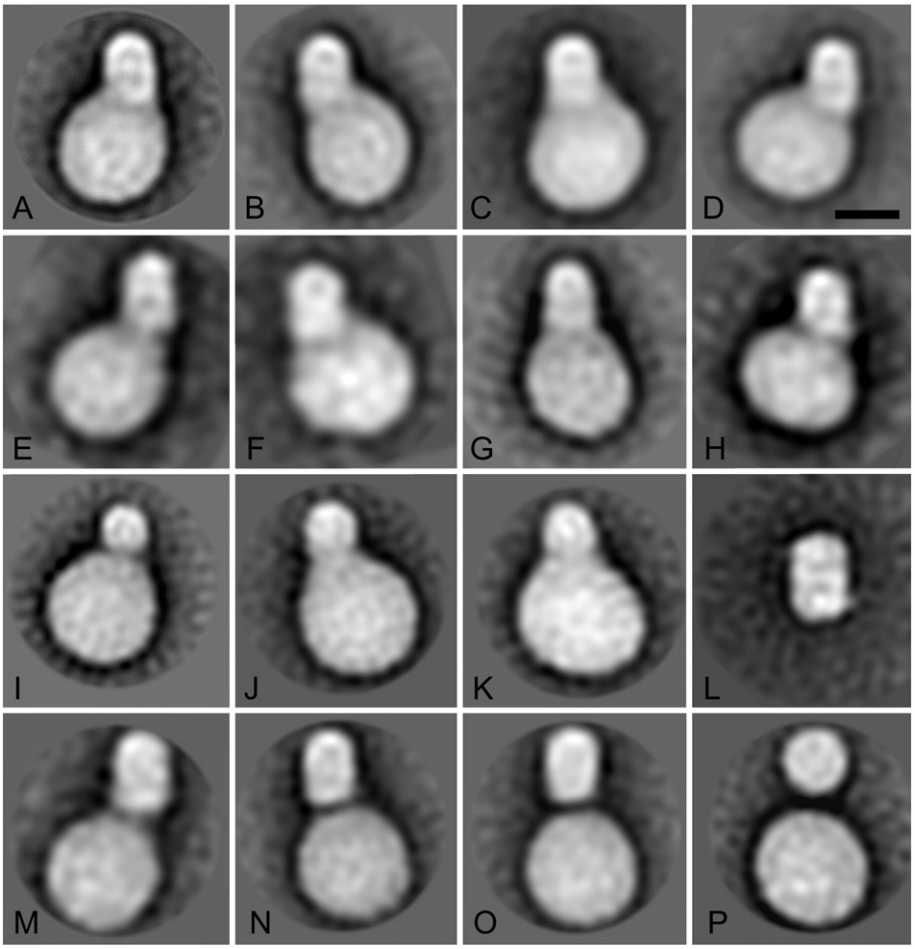

Fig. 3. Projection maps of *Arabidopsis* PSI-Cytb$_6$f supercomplexes, obtained by single particle electron microscopy. (A–H) Supercomplexes composed of PSI and dimeric Cytb$_6$f complex in different orientations. (I–K) Supercomplexes binding monomeric Cytb$_6$f complex in different orientations. (L) Map of dimeric Cytb$_6$f complex. (M–O) Maps of supercomplexes with a loosely bound Cytb$_6$f dimer in positions about equivalent to those shown in frames A–C. (P) Map of a PSI complex with a fully separated Cytb$_6$f complex. Maps contain on average about 400 summed particles. The scale bar is 100 Å.

LHCII supercomplex was the most common particle in the FFE fractions 48–49 (Fig. 5A). Interestingly, particles of double size were present in low frequency, and image analysis showed indeed that PSI-LHCII supercomplexes can dimerize (Fig. 5B). FFE fractions also contained particles resembling the standard PSI-LHCII particle, but with additional extensions. The map of one of these particles, comprised of over 600 projections indicated that the additional density has the size and shape of a LHCII trimer (Fig. 5C) and modelling of the atomic models of PSI and LHCII into this PSI-LHCII$_2$ supercomplex map indicates that the second LHCII trimer was attached to Lhca2 and Lhca4 antenna subunits (Fig. 7D). In another supercomplex, similar to PSI-LHCII$_2$ (Fig. 5C), the second LHCII trimer attached to the Lhca2 and Lhca3 antenna subunits (Fig. 5D). Two similar maps may represent the same particle in a slightly tilted situation (Fig. 5E, F).

3.3. Analysis of Arabidopsis PSI-NDH supercomplexes

The discovery of novel PSI-LHCII supercomplexes raised the question about the existence of supercomplexes larger than the ones composed of NDH and 1–2 copies of PSI, as found in a previous study in barley [3]. Indeed, a former biochemical analysis indicated that NDH might associate with up to three copies of PSI [30]. FFE fractions enriched in PSI lacked substantial numbers of PSI-NDH supercomplexes necessary for a refined analysis by single particle EM. Nevertheless, our recent search for large molecular assemblies in mildly solubilized thylakoid membranes from *Arabidopsis thaliana* using CN-PAGE revealed, in addition to large PSII megacomplexes [18], the presence of large variable associations between NDH complex and multiple copies of PSI. A batch of PSI-NDH supercomplexes with a total number of 35,000 particles was analyzed. As a result, a wealth of novel information was obtained. Besides the previously found supercomplexes with one or two PSI

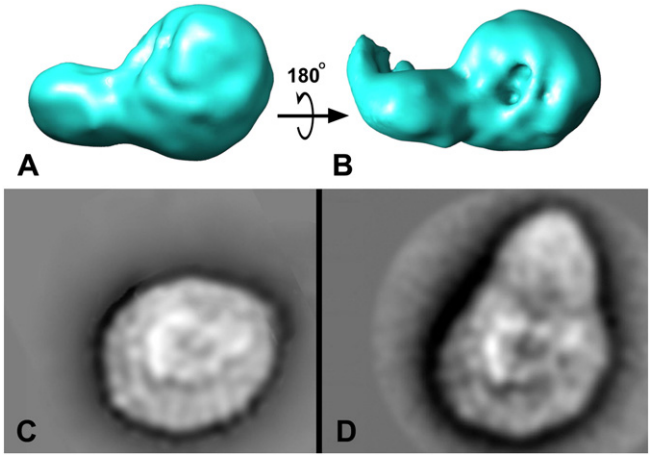

Fig. 4. Assignment of the position of Cytb$_6$f in the *Arabidopsis* PSI-Cytb$_6$f supercomplex. (A) Three-dimensional model of the PSI-Cytb$_6$f supercomplex, seen from the stromal side with the Cytb$_6$f complex at the left side of the PSI complex, as shown in C. (B) Model of the PSI-Cytb$_6$f supercomplex seen from the lumenal side. (C) Low-pass filtered 2D map of the regular PSI complex, in a position similar to the PSI-Cytb$_6$f supercomplex model. (D) Map of the PSI-LHCII supercomplex [2,5].

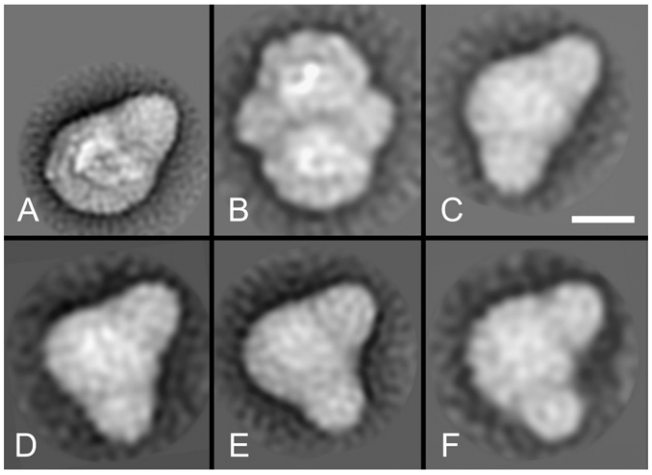

Fig. 5. Projection maps of PSI-LHCII supercomplexes, obtained from single particle image processing. (A) PSI-LHCII supercomplex. (B) Dimeric PSI-LHCII supercomplex, with the lower part in a position as in frame A. (C) PSI-LHCII$_2$ supercomplex with a second LHCII trimer attached to the Lhca2 and Lhca4 antenna subunits. (D–F) Similar maps of a PSI-LHCII supercomplex with the second LHCII trimer attached to the Lhca2 and Lhca3 antenna subunits. The particles may differ mostly in a tilt out of the membrane plane. The scale bar is 100 Å.

complexes flanking NDH (Fig. 6A,B), three other types of PSI-NDH particles that can bind additional copies of PSI on one side were identified (Fig. 6C–F). If all possible maps are combined, NDH can, hypothetically, associate with 5 PSI complexes on one side, as schematically outlined (Fig. 6G). Indeed, a PSI cluster containing 5 copies, but without NDH, was found (Fig. 6H). In this cluster, the PSI complexes are proposed to be organized at positions according to the model (Fig. 6G).

Another intriguing aspect is that the NDH complex from Arabidopsis, although strongly related to NDH-1 from cyanobacteria, appeared to be similar to mitochondrial Complex I, which has a much higher number of additional subunits than NDH-1. In tilted views or side view positions, the protrusions of NDH, attached to the membrane-bound arm, are visible in a non-overlap position (Fig. 6I,K, red arrowheads). These protrusions, as seen in the side view map (Fig. 6L) are remarkably similar to those of plant Complex I (Fig. 6M). It is tempting to see this as a mistaking exchange, but it should be noted that the protrusions are also visible if PSI still connected (Fig. 6I) and that on the other side plant Complex I, as studied by Peters and coworkers, was partially connected to Complex III, an unmistaken component of a mitochondrial supercomplex [31].

4. Discussion

In this study, supercomplexes of PSI were isolated that may be discussed as a structural basis for the regulation of CEF in the non-stacked thylakoid membrane. The structures of PSI [28,29], the Cytb$_6$f complex [25,26,32], and NDH complex [33] have been characterized, and chemical steps in energy trapping [34] and electron transfer via iron-sulfur centers are known in detail. However, less is known about the structural arrangement of the complexes in the non-stacked chloroplast membrane and the functional role of supercomplexes composed of these components in regulation of CEF. Clear evidence for structural arrangement of two PSI with NDH in a supercomplex has been shown [3]. Despite the claims for the elusive PSI-Cytb$_6$f supercomplex in the green alga *Chlamydomonas reinhardtii* [14], no progress has been published regarding purification and subsequent structural characterization of its counterpart in green plants. Several types of particles were characterized in an extensive survey of PSI supercomplexes in non-stacked chloroplast membranes, but none of them had Cytb$_6$f attached [35]. Apparently the interaction between PSI and Cytb$_6$f is very loose and can be easily disrupted by detergents during purification.

In this work we have pursued the structural characterization of elusive PSI supercomplexes in two ways: (1) we pushed the collection of single particle projections to the limit by recording about 100,000 EM

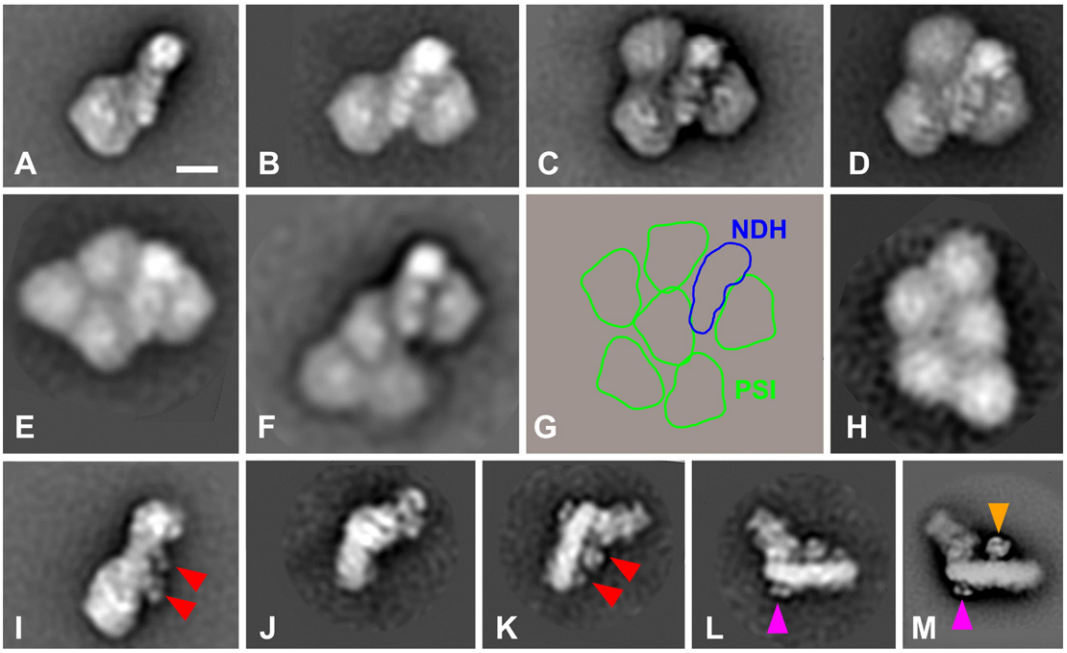

Fig. 6. Analysis of PSI-NDH supercomplexes from Arabidopsis. (A) Map of the PSI$_1$-NDH supercomplex. (B) Map of the PSI$_2$-NDH supercomplex. (C) Map of the PSI$_3$-NDH supercomplex. (D) Map of the PSI$_3$-NDH supercomplex in a slightly tilted position, in which the upper left PSI complex becomes larger in projection and the right PSI complex smaller.(E) Map of a PSI$_4$-NDH supercomplex. (F) Map of another PSI$_4$-NDH supercomplex. (G) Schematic model for the largest possible PSI$_6$-NDH supercomplex with 5 copies of PSI attached at the left and one at the right. (H) Particle consisting of 5 PSI complexes, in positions as in the model. (I) Map of NDH-PSI$_1$ in a tilted position, protruding densities of the NDH part are indicated by red arrowheads. (J) NDH complex in a tilted position, protrusions are not visible, the hydrophilic arm is partially in a non-overlap position with the membrane domain. (K) NDH in side-view position, with protrusions as in frame I marked by red arrowheads. (L) Same map as in frame J, shifted in a horizontal position. (M) Map of mitochondrial Complex I (reproduced from [31]. Orange arrowhead point to the attached Carbonic anhydrase. Purple arrowheads in frames L and M point to a characteristic density present in both chloroplast NDH and mitochondrial Complex I, and named P2 in the latter. Scale bar is 100 Å.

micrographs of potential PSI-Cytb$_6$f supercomplexes and other supercomplexes. Large data sets of single particle projections, obtained by manual picking and semi-automated extractions from these images, were submitted to single particle averaging, including automated classification. (2) We used free-flow electrophoresis for separation of the complexes. The approach avoids typical problems associated with gel-electrophoresis like size filtration, artificial charge shift, and high in-gel concentration of proteins especially at the liquid gel junction. Protein complexes are separated based on the pH dependent native charge of the complexes and resolution is achieved by mobility differences in defined interval pH zones (Fig. 1). A concentration of complexes in bands is achieved at pH steps during the separation process. A typical separation of all solubilized membrane protein complexes is achieved in parallel within about 4–6 min. Potential fractions of PSI-Cytb$_6$f and other supercomplexes were selected in the isolation buffer after spectroscopic screening and additional biochemical examinations of the FFE fractions. In this combined way, new supercomplexes were found, which are discussed below.

4.1. PSI-LHCII in Arabidopsis

In a previous study the PSI-LHCII supercomplex was purified by sucrose gradient fractionation and only one particle was found, consisting of a PSI complex and one LHCII trimer [5]. No larger particles were present. The use of free-flow electrophoresis provides an access to the solubilized complexes within minutes. (Labile) supercomplexes could therefore be analyzed much faster, which appears beneficial to characterization. On the other side, the lower resolution of the one-step purification strategy results in some heterogeneity in the obtained fractions. This was evident from the detection of low amounts of proteins originating from complexes with similar molecular weight by MS analysis after native BN-PAGE and was also evident during inspection by EM. However, in the structural characterization the problem of heterogeneity can be circumvented to a large extent. Extensive sorting of projections by statistical analysis has been applied during the structural analysis by single particle EM. In this way we could separate the projection maps belonging to different types of particles.

In the free-flow fractions several types of larger PSI-LHCII supercomplexes were found and homogeneous 2D projection maps were obtained by image processing of large numbers of EM projections (Fig. 5). For the first time dimers of PSI-LHCII particles were detected, which we propose to name PSI$_2$-LHCII$_2$ (Fig. 5B). Further, PSI-LHCII particles which contain an additional LHCII trimer in two slightly different positions were revealed (Fig. 5C and D). The position indicates that the additional LHCII trimer is connected to the PSI core part either via the peripheral antenna subunits Lhca2/Lhca3 or Lhca4/Lhca2 (Figs. 5C and D, 7D). In the first case, the lumenal PsaN subunit, located next to Lhca3 [28], might also be involved in the binding. The finding of PSI complexes with two LHCII trimers, which we propose to name PSI-LHCII$_2$, is not totally unexpected. It was recently suggested from biochemical experiments that PSI binds more than one LHCII trimer [36,37]. In conclusion, the novel PSI-LHCII$_2$ supercomplexes suggest that the interaction with the peripheral LHCII antenna is more complex than previously considered. Therefore, the current view that part of the mobile fraction of LHCII moves towards PSI and binds at only one specific site under state transition [5], should be revised.

4.2. PSI-Cytb$_6$f in Arabidopsis

The comparison of the 3D model of Arabidopsis PSI-Cytb$_6$f supercomplex with existing 2D maps of known orientation clearly indicates one unique binding site of Cytb$_6$f to PSI, next to the peripheral antenna subunit Lhca1 (Fig. 7). The Cytb$_6$f complex binds as a monomer or dimer, although only the dimer is considered to be the active form [34]. There is no clear evidence that any other additional protein is binding to the PSI-Cytb$_6$f supercomplex, but given the low resolution of the maps and model, which is around 30 Å, association of other small proteins cannot be ruled out. There is no indication in *Arabidopsis* for the elusive supercomplex between PSI, Cytb$_6$f, LHCII, FNR and PGRL1, proposed some years ago for *Chlamydomonas* [14]. But in principle, the binding of Cytb$_6$f to Lhca1 would not prevent binding of a LHCII trimer to Lhca2–4. Interestingly, the Cytb$_6$f dimer associates with its short side rather than its long side to PSI. This way of binding could explain why PSI-Cytb$_6$f particles are prone to dissociation and are present in low abundance, even if analysis is performed about an hour after their solubilization, as in this study. The small protein plastocyanin functions as an electron transporter between the cytochrome f subunit of Cytb$_6$f and PSI. In the way that Cytb$_6$f and PSI associate in the supercomplex, this distance is relatively small (black circles, Fig. 7A). This could be a reason why the PSI-Cytb$_6$f supercomplex has this particular shape, as further discussed in Section 4.4.

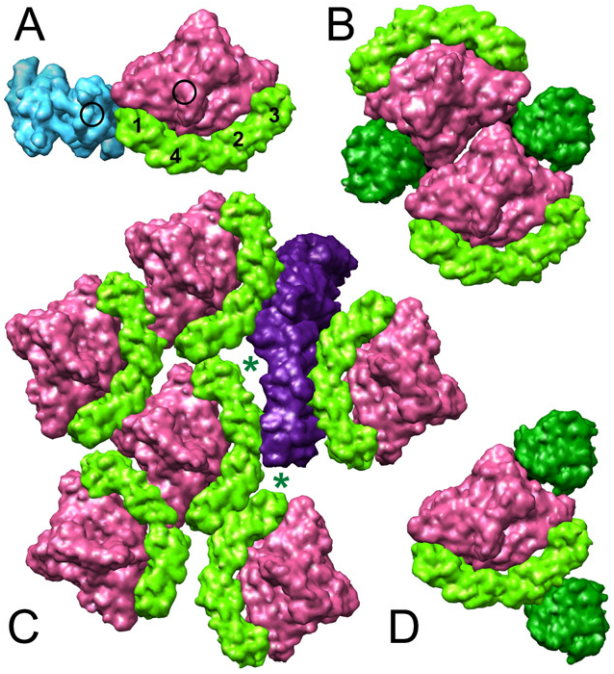

Fig. 7. Models of the PSI supercomplexes. (A) *Arabidopsis* PSI-Cytb$_6$f model, with the PSI core part in purple, LHCI in bright green and Cytb$_6$f in blue. The position of the Lhca1–4 subunits is indicated by numbers, plastocyanin-binding regions are indicated with black circles. (B) Dimeric PSI-LHCII complex. (C) Largest type of PSI-NDH supercomplex; the open space (green asterisks) could according to [3] be occupied by the Lhca5/6 antenna subunits. (D) *Arabidopsis* PSI-LHCII$_2$ complex, with a second LHCII trimer (dark green) attached to Lhca2/3. From the models all high-resolution components have been filtered to 10 Å, to avoid overinterpretation.

4.3. PSI-NDH in Arabidopsis

The extended analysis of PSI-NDH complexes revealed that NDH can bind up to 6 PSI complexes. This number is higher than the 1–2 PSI complexes found earlier in barley [3,33]. This likely means that NDH is able to make specific clusters with PSI. We identified low amounts of these clusters, but without NDH (Fig. 6H). Clusters of PSI are novel, because earlier attempts to extract PSI multimers ended up in artificial detergent-induced aggregates in which the particles were oriented both upside-up and upside-down [4]. It is possible that the low-abundant Lhca5 and 6 antenna subunits function in pasting the PSI complexes to NDH, as discussed earlier [3]. The EM maps do not have enough detail to see such proteins, but according to the modeling there is enough open space available to put in Lhca5 and 6 (green asterisks, Fig. 7C). Of the two subunits, Lhca5 was found to be present in the NDH band by MS analysis (not shown).

There is one intriguing aspect about the analysis of supercomplexes, although not directly related to the main issue of this work about PSI interactions. We can now compare NDH, as bound to PSI, with mitochondrial Complex I, as a single entity or as bound to Complex III in supercomplexes [31]. The chloroplast NDH complex strongly resembles the mitochondrial complex (Fig. 6L, M), although they are not closely related from a sequence perspective. It is striking that NDH from *Arabidopsis* contains a central protrusion, just as in Complex I (orange arrowhead in Fig. 6M). This protrusion was determined in plant mitochondria as the carbonic anhydrase domain, functional in carbon metabolism [38]. Chloroplast NDH is composed of about 30 subunits [39,40] and mitochondrial Complex I has over 40 subunits [41], of which many have an unknown function. This may explain the similarity. The striking resemblance of chloroplast NDH and mitochondrial Complex I needs further attention, the more because the origin of the particles studied is incontrovertible. PSI and Complex III are specific for chloroplasts and mitochondria, respectively, and each complex has a unique, and easily recognizable shape.

4.4. Function of spatial separation of PSI, Cytb$_6$f and NDH

The structural organization of the thylakoid membrane has been often studied, but investigations mostly deal with stacked grana membranes, where PSII often forms semi-crystalline arrays [1,42]. It also the non-stacked grana membrane is largely composed of PSI, Cytb$_6$f, and ATP synthase, and besides these proteins it is considered to accommodate monomeric PSII complexes and single trimers of LHCII [43]. It is not known how all these components interact. The last years have shown that PSI is undoubtedly a key protein in the regulation of electron flow. One important reason is its multiple functions in capturing energy. PSI is involved in LEF and two types of CEF to modulate the ATP: NADPH production and in reaction to stress phenomena. PSI uses light energy to mediate electron transfer from plastocyanin to ferredoxin. Next, ferredoxin transports electrons from PSI to FNR in LEF or to either Cytb$_6$f or NDH in CEF. This electron transport via plastocyanin and ferredoxin is diffusion limited. This implies that regulation of the distances by structural alignment of PSI with NDH or with Cytb$_6$f can control the electron transfer kinetics. We hypothesize that by the tuning of distances from PSI to NDH and Cytb$_6$f in supercomplexes and/or small domains the two known types of CEF can be differentiated. How this is performed in detail is not yet clear. One reason is that small but essential components of the two types of CEF, such as PGRL1 and PGRL5, could not be established.

Interestingly, small domains that may facilitate CEF in the non-stacked grana appear to have a counterpart in the stacked grana membrane. Recently, nanodomains of colocalized PSII and Cytb$_6$f complexes were found by AFM and it was suggested that the close proximity between PSII and Cytb6f complexes fosters the short-range diffusion of plastoquinone in the membrane [44]. But there is no indication that PSII forms supercomplexes with Cytb$_6$f and it also needs to be established to what extend close proximity of PSII and Cytb6f is beneficial for LEF.

In conclusion, the novel types of supercomplexes, described in this study, imply further that the non-stacked grana membrane has a higher level of organization than previously considered. The structural data on supercomplexes clearly provide a framework for further research in the regulation of PSI, as part of the primary reactions in plant photosynthesis.

Transparency document

The Transparency document associated with this article can be found, in online version.

Acknowledgements

We thank Dr. G. Weber, and Mrs. U. Sukop-Köppel (FFE Service GmbH, Germany) for support with free-flow electrophoresis. Work at University of Groningen was supported by NWO Chemical Sciences. Work at Palacký University was supported by a Marie Curie Career Integration Grant call FP7-PEOPLE-2012-CIG (322193 to RK) and by grant LO1204 (Sustainable development of research in the Centre of the Region Haná to RK) from the National Program of Sustainability I from the Ministry of Education, Youth and Sports, Czech Republic. Work at the University of Stavanger was supported by NFR 240770.

Appendix A. Supplementary data

Supplementary data to this article can be found online at doi:10.1016/j.bbabio.2016.10.006.

References

[1] R. Kouřil, J.P. Dekker, E.J. Boekema, Supramolecular organization of photosystem II in green plants, Biochim. Biophys. Acta 117 (2012) 2–12, http://dx.doi.org/10.1016/j.bbabio.2011.05.024.
[2] R. Kouřil, A. Zygadlo, A.A. Arteni, C.D. de Wit, J.P. Dekker, P.E. Jensen, H.V. Scheller, E.J. Boekema, Structural characterization of a complex of photosystem I and light-harvesting complex II of *Arabidopsis thaliana*, Biochemistry 44 (2005) 10935–10940, http://dx.doi.org/10.1021/bi051097a.
[3] R. Kouřil, O. Strouhal, L. Nosek, R. Lenobel, I. Chamrad, E. Boekema, M. Sebela, P. Ilik, Structural characterization of a plant photosystem I and NAD(P)H dehydrogenase supercomplex, Plant J. 77 (2014) 568–576, http://dx.doi.org/10.1111/tpj.12402.
[4] R. Kouřil, N. van Oosterwijk, A.E. Yakushevska, E.J. Boekema, Photosystem I: a search for green plant trimers, Photochem. Photobiol. Sci. 4 (2005) 1091–1094, http://dx.doi.org/10.1039/b505519a.
[5] P. Galka, S. Santabarbara, T.T.H. Khuong, H. Degand, P. Morsomme, R.C. Jennings, E.J. Boekema, S. Caffari, Functional analyses of the plant photosystem I–light-harvesting complex II supercomplex reveal that light-harvesting complex II loosely bound to photosystem II is a very efficient antenna for photosystem I in state II, Plant Cell 24 (2012) 2963–2978, http://dx.doi.org/10.1105/tpc.112.100339.
[6] B. Drop, K.N.S. Yadav, E.J. Boekema, R. Croce, Consequences of state transitions on the structural and functional organization of photosystem I in the green alga *Chlamydomonas reinhardtii*, Plant J. 78 (2014) 181–191, http://dx.doi.org/10.1111/tpj.12459.
[7] G.N. Johnson, Physiology of PSI cyclic electron transport in higher plants, Biochim. Biophys. Acta 1807 (2011) 384–389, http://dx.doi.org/10.1016/j.bbabio.2010.11.009.
[8] G. DalCorso, P. Pesaresi, S. Masiero, E. Aseeva, D. Schünemann, G. Finazzi, P. Joliot, R. Barbato, D. Leister, A complex containing PGRL1 and PGR5 is involved in the switch between linear and cyclic electron flow in Arabidopsis, Cell 132 (2008) 273–285, http://dx.doi.org/10.1016/j.cell.2007.12.028.
[9] P.A. Burrows, L.A. Sazanov, Z. Svab, P. Maliga, P.J. Nixon, Identification of a functional respiratory complex in chloroplasts through analysis of tobacco mutants containing disrupted plastid ndh genes, EMBO J. 17 (1998) 868–887, http://dx.doi.org/10.1093/emboj/17.4.868.
[10] T. Shikanai, T. Endo, T. Hashimoto, Y. Yamada, K. Asada, A. Yokota, Directed disruption of the tobacco ndhB gene impairs cyclic electron flow around photosystem I, Proc. Natl. Acad. Sci. U. S. A. 95 (1998) 9705–9709.
[11] Y. Munekage, M. Hashimoto, C. Miyake, K.I. Tomizawa, T. Endo, M. Tasaka, T. Shikanai, Cyclic electron flow around photosystem I is essential for photosynthesis, Nature 429 (2004) 579–582, http://dx.doi.org/10.1038/nature02598.
[12] A.K. Livingston, J.A. Cruz, K. Kohzuma, A. Dhingra, D.M. Kramer, An Arabidopsis mutant with high cyclic electron flow around photosystem I (hcef) involving the NADPH dehydrogenase complex, Plant Cell 22 (2010) 221–233, http://dx.doi.org/10.1105/tpc.109.071084.
[13] L.M. Casano, M. Martín, B. Sabater, Hydrogen peroxide mediates the induction of chloroplastic Ndh complex under photooxidative stress in barley, Plant Physiol. 125 (2001) 1450–1458.
[14] M. Iwai, K. Takizawa, R. Tokutsu, A. Okamura, Y. Takahashi, J. Minagawa, Isolation of the elusive supercomplex that drives cyclic electron flow in photosynthesis, Nature 464 (2010) 1210–1213, http://dx.doi.org/10.1038/nature08885.
[15] A. Shapiguzov, B. Ingelsson, I. Samol, C. Andres, F. Kessler, J.D. Rochaix, A.V. Vener, M. Goldschmidt-Clermont, The PPH1 phosphatase is specifically involved in LHCII dephosphorylation and state transitions in Arabidopsis, Proc. Natl. Acad. Sci. U. S. A. 107 (2010) 4782–4787, http://dx.doi.org/10.1073/pnas.0913810107.
[16] H. Takahashi, S. Clowez, F.A. Wollman, O. Vallon, F. Rappaport, Cyclic electron flow is redox-controlled but independent of state transition, Nat. Commun. 4 (2013), 1954, http://dx.doi.org/10.1038/ncomms2954.
[17] L.A. Eichacker, G. Weber, U. Sukop-Köppel, R. Wildgruber, Free flow electrophoresis for separation of native membrane protein complexes, Methods Mol. Biol. 1295 (2015) 415–425, http://dx.doi.org/10.1007/978-1-4939-2550-6_29.
[18] L. Nosek, D. Semchonok, E.J. Boekema, P. Ilik, R. Kouřil, Structural variability of plant photosystem II megacomplexes in thylakoid membranes, Plant J. (2016), http://dx.doi.org/10.1111/tpj.13325 (in press).
[19] V. Reisinger, L.A. Eichacker, Solubilization of membrane protein complexes for blue native PAGE, J. Proteome 71 (2008) 277–283, http://dx.doi.org/10.1016/j.jprot.2008.05.004.

[20] D. Kang, Y.S. Gho, M. Suh, C. Kang, Highly sensitive and fast protein detection with Coomassie brilliant blue in sodium dodecyl sulfate-polyacrylamide gel electrophoresis, Bull. Kor. Chem. Soc. 23 (2002) 1511–1512, http://dx.doi.org/10.5012/bkcs.2002.23.11.1511.
[21] S.H.W. Scheres, R. Núñez-Ramírez, C.O. Sorzano, J.M. Carazo, R. Marabini, Exploring the conformational flexibility of macromolecular machines, Nat. Protoc. 3 (2008) 977–990, http://dx.doi.org/10.1038/nprot.2008.62.
[22] S.H.W. Scheres, A Bayesian view on cryo-EM structure determination, J. Mol. Biol. 415 (2012) 406–418, http://dx.doi.org/10.1016/j.jmb.2011.11.010.
[23] J.M. de la Rosa-Trevín, A. Quintana, L. Del Cano, A. Zaldívar, I. Foche, J. Gutiérrez, J. Gómez-Blanco, J. Burguet-Castell, J. Cuenca-Alba, V. Abrishami, J. Vargas, J. Otón, G. Sharov, J.L. Vilas, J. Navas, P. Conesa, M. Kazemi, R. Marabini, C.O.S. Sorzano, J.M. Carazo, Scipion: a software framework toward integration, reproducibility and validation in 3D electron microscopy, J. Struct. Biol. 195 (2016) 93–99, http://dx.doi.org/10.1016/j.jsb.2016.04.010.
[24] E.J. Boekema, G. Schmidt, P. Gräber, J. Berden, Structure of the ATP-synthase from chloroplasts and mitochondria studied by electron microscopy, Z. Naturforsch. 43C (1988) 219–225.
[25] D. Stroebel, Y. Choquet, J.-L. Popot, D. Picot, An atypical haem in the cytochrome b6f complex, Nature 426 (2003) 413–418, http://dx.doi.org/10.1038/nature02155.
[26] G. Kurisu, H. Zhang, J.L. Smith, W.A. Cramer, Structure of the cytochrome b6f complex of oxygenic photosynthesis: tuning the cavity, Science 302 (2003) 1009–1014, http://dx.doi.org/10.1126/science.1090165.
[27] G. Mosser, C. Breyton, A. Olofsson, J.L. Popot, J.L. Rigaud, Projection map of cytochrome b6f complex at 8 Å resolution, J. Biol. Chem. 272 (1997) 20263–20268.
[28] A. Amunts, O. Drory, N. Nelson, The structure of a plant photosystem I supercomplex at 3.4 Å resolution, Nature 447 (2007) 58–63, http://dx.doi.org/10.1038/nature05687.
[29] Y. Mazor, A. Borovikova, N. Nelson, The structure of plant photosystem I supercomplex at 2.8 Å resolution, eLife 4 (2015) e07433, http://dx.doi.org/10.7554/eLife.07433.
[30] L. Peng, H. Shimizu, T. Shikanai, The chloroplast NAD(P)H dehydrogenase complex interacts with photosystem I in Arabidopsis, J. Biol. Chem. 283 (2008) 34873–34879, http://dx.doi.org/10.1074/jbc.M803207200.
[31] K. Peters, N.V. Dudkina, L. Jänsch, H.P. Braun, E.J. Boekema, A structural investigation of complex I and I + III2 supercomplex from *Zea mays* at 11-13 Å resolution: assignment of the carbonic anhydrase domain and evidence for structural heterogeneity within complex I, Biochim. Biophys. Acta 1777 (2008) 84–93, http://dx.doi.org/10.1016/j.bbabio.2007.10.012.
[32] D. Baniulis, E. Yamashita, H. Zhang, S.S. Hasan, W.A. Cramer, Structure-function of the cytochrome b6f complex, Photochem. Photobiol. 84 (2008) 1349–1358, http://dx.doi.org/10.1111/j.1751-1097.2008.00444.x.
[33] L. Peng, T. Shikanai, Supercomplex formation with photosystem I is required for the stabilization of the chloroplast NADH dehydrogenase-like complex in Arabidopsis, Plant Physiol. 155 (2011) 1629–1639, http://dx.doi.org/10.1104/pp.110.171264.
[34] R. Croce, H. van Amerongen, Light-harvesting in photosystem I, Photosynth. Res. 116 (2013) 153–166, http://dx.doi.org/10.1007/s11120-013-9838-x.
[35] M. Suorsa, M. Rantala, F. Mamedov, M. Lespinasse, A. Trotta, M. Grieco, E. Vuorio, M. Tikkanen, E. Jarvi, E.M. Aro, Light acclimation involves dynamic re-organization of the pigment-protein megacomplexes in non-appressed thylakoid domains, Plant J. 84 (2015) 360–373, http://dx.doi.org/10.1111/tpj.13004.
[36] A.J. Bell, L.K. Frankel, T.M. Bricker, High yield non-detergent isolation of photosystem I-light-harvesting chlorophyll II membranes from spinach thylakoids: implications for the organization of the PS I antennae in higher plants, J. Biol. Chem. 290 (2015) 18429–31847, http://dx.doi.org/10.1074/jbc.M115.663872.
[37] S.L. Benson, P.M. Maheswaran, M.A. Ware, C.N. Hunter, P. Horton, S. Jansson, A.V. Ruban, M.P. Johnson, An intact light harvesting complex I antenna system is required for complete state transitions, Nat. Plants 1 (2015), 15176, http://dx.doi.org/10.1038/nplants.2015.176.
[38] S. Sunderhaus, N.V. Dudkina, L. Jänsch, J. Klodmann, J. Heinemeyer, M. Perales, E. Zabaleta, E.J. Boekema, H.P. Braun, Carbonic anhydrase subunits form a matrix-exposed domain attached to the membrane arm of mitochondrial complex I in plants, J. Biol. Chem. 281 (2006) 6482–6488, http://dx.doi.org/10.1074/jbc.M511542200.
[39] K. Ifuku, T. Endo, T. Shikanai, E.M. Aro, Structure of the chloroplast NADH dehydrogenase-like complex: nomenclature for nuclear-encoded subunits, Plant Cell Physiol. 52 (2011) 1560–1568, http://dx.doi.org/10.1093/pcp/pcr098.
[40] T. Shikanai, Chloroplast NDH: a different enzyme with a structure similar to that of respiratory NADH dehydrogenase, Biochim. Biophys. Acta 1857 (2016) 1015–1022, http://dx.doi.org/10.1016/j.bbabio.2015.10.013.
[41] E.H. Meyer, Proteomic investigations of complex I composition: how to define a subunit? Front. Plant Sci. 3 (2012), 106, http://dx.doi.org/10.3389/fpls.2012.00106.
[42] H. Kirchhoff, Diffusion of molecules and macromolecules in thylakoid membranes, Biochim. Biophys. Acta 1837 (2014) 495–502, http://dx.doi.org/10.1016/j.bbabio.2013.11.003.
[43] J.P. Dekker, E.J. Boekema, Supermolecular organization of the thylakoid membrane proteins in green plants, Biochim. Biophys. Acta 1706 (2005) 12–39, http://dx.doi.org/10.1016/j.bbabio.2004.09.009.
[44] M.P. Johnson, C. Vasilev, J.D. Olsen, C.N. Hunter, Nanodomains of cytochrome b_6f and photosystem II complexes in spinach grana thylakoid membranes, Plant Cell 26 (2014) 3051–3061, http://dx.doi.org/10.1105/tpc.114.127233.